ISSN 1063-7761, Journal of Experimental and Theoretical Physics, 2009, Vol. 109, No. 2, pp. 280–285. © Pleiades Publishing, Inc., 2009.
Original Russian Text © L.Ya Vinnikov, D.É. Boĭnagrov, V.N. Zverev, I.S. Veshchunov, J. Karpinski, 2009, published in Zhurnal Éksperimental'noĭ i Teoreticheskoĭ Fiziki, 2009, Vol. 136, No. 2, pp. 331–337.

ELECTRONIC PROPERTIES OF SOLID

Anisotropy of the Vortex Structure and Resistivity in the Basal Plane of $YBa_2Cu_4O_8$ Single Crystals

L. Ya Vinnikov[a], D. É. Boĭnagrov[a], V. N. Zverev[a], I. S. Veshchunov[a], and J. Karpinski[b]

[a] *Institute of Solid State Physics, Russian Academy of Sciences, Chernogolovka, Moscow oblast, 142432 Russia*

[b] *Laboratory for Solid State Physics, ETH Zurich 8093, Zurich, Switzerland*

e-mail: vinnik@issp.ac.ru

Received December 30, 2008

Abstract—The vortex lattice of the $YBa_2Cu_4O_8$ high-temperature superconductor is studied in the basal plane of monocrystalline samples using the decoration technique in a field interval of 40–600 Oe. Vortex lattice anisotropy (field-independent "compression" of a regular hexagonal vortex cell in the poorly conducting direction by a factor of about 1.3) is detected. Resistivity anisotropy ρ_a/ρ_b measured at temperatures from T_c to room temperature is 16–9. Possible reasons for the discrepancy between our results and the available data are discussed.

PACS numbers: 71.18.+y, 74.25.Qt, 74.72.Bk

DOI: 10.1134/S1063776109080135

1. INTRODUCTION

Single crystals of the $YBa_2Cu_4O_8$ high-temperature superconductor (HTSC) exhibit noticeable anisotropy of properties in the *ab* basal plane due to the position of oxygen in double chains (along the **b** axis of the orthorhombic crystal structure) [1–3]. The interest in this compound is associated with analysis of how properties in the normal state affect superconductivity and with the fact that these single crystals are simultaneously stoichiometric, underdoped, and contain no twins in contrast to $YBa_2Cu_3O_{7-x}$ [4–7]. In recent years, this interest has been heated by the study of natural (intrinsic) inhomogeneity of HTSCs [8]. Optical and resistive measurements in the basal plane revealed anisotropy in resistivity, which is the strongest in directions **a** and **b** [2]. This should lead to corresponding anisotropy in penetration depth λ and its manifestation in the vortex structure analogously to $YBa_2Cu_3O_7$ single crystals [9]. Imperfections (pinning centers) of a real crystal must undoubtedly affect the formation of the vortex structure [10].

A theoretical description of distortion in a regular triangular Abrikosov vortex lattice in the absence of pinning in the anisotropic case is based on allowance for the effective mass tensor in the Ginzburg–Landau equations in the London approximation [11, 12], in which the ratio $(b/\lambda)^2 \ll 1$ is a small parameter and b and λ are the mean values of the parameters. This means that the solution corresponds to the condition of observation of the vortex structure in the field interval $H_{c1} \ll H \ll H_{c2}$.

It was shown in [11] that a regular triangular lattice in the isotropic case (the unit cell is constructed on vectors $\mathbf{b}_1$ and $\mathbf{b}_2$ so that $|\mathbf{b}_1| = |\mathbf{b}_2|$ and angle φ between these vectors is 60°) is transformed in the anisotropic case into a rhombic unit cell with $\varphi \neq 60°$ (in our case, vectors $\mathbf{b}_1$ and $\mathbf{b}_2$ lie in the basal plane; see Fig. 1). The following relation was derived in [11]:

$$2b_2/b_1 = (1 + 3M_a/M_b)^{0.5}, \quad (1)$$

where M_a and M_b are the effective masses in directions **a** and **b**, respectively; $(M_a/M_b)^{0.5} = 1/\varepsilon$ in the notation

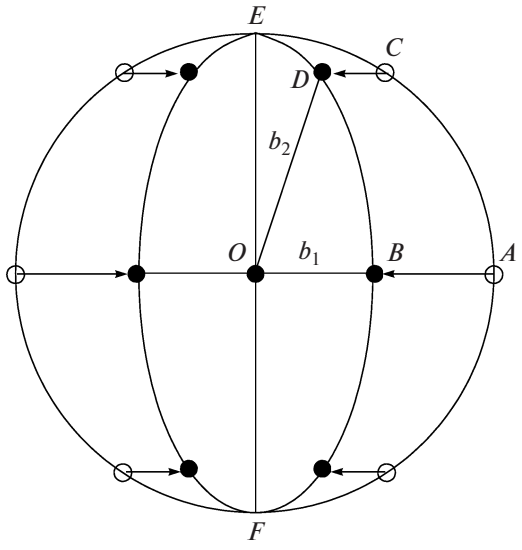

Fig. 1. Diagram of transformation of a regular triangular vortex lattice in the basal plane in a tetragonal ($a = b$) and orthorhombic ($a \neq b$) crystals.

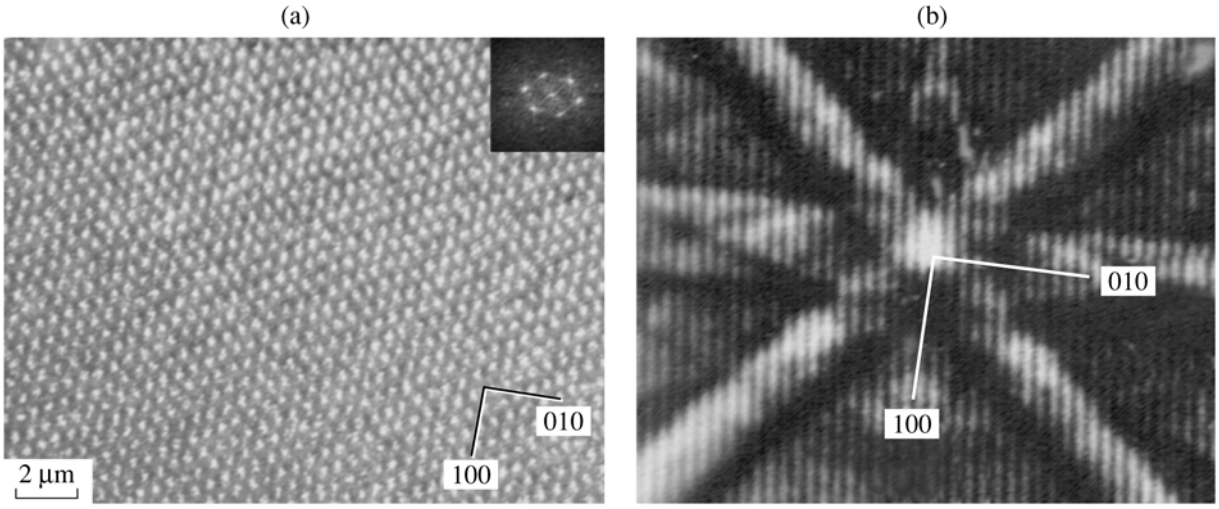

Fig. 2. (a) Vortex lattice in the basal plane of a $YBa_2Cu_4O_8$ single crystal in a magnetic field of 41 Oe and (b) electron channeling pattern for the same microscopic region in the single crystal.

adopted in [12]. Uniform (in the **a** direction) compression, by a factor of $\eta = 1/\varepsilon$, of a circle passing through the sites of a regular triangular lattice results in an ellipse in the anisotropic case. This elliptic curve contains the sites of the anisotropic vortex lattice formed in this way with a new basis $\mathbf{b}_1$, $\mathbf{b}_2$. The ratio of semiaxes of the ellipse is $A/B = \eta = 1/\varepsilon$, where A and B are the length of the major and minor semiaxes.

Simple geometrical analysis of the pattern (Fig. 1) shows that the relation between the vectors of an isotropic lattice with coordinates of the tips of the vectors at points $A(b_1, 0)$ and $C(b_1/2, b_1\sqrt{3/2})$ and an anisotropic lattice compressed by a factor of $1/\varepsilon$ in the direction of the abscissa with coordinates $B(b_1, 0)$ and $D(b\varepsilon/2, b_1\sqrt{3/2})$ leads to relation (1). Indeed, it can be seen from Fig. 1 that segment BD is given by

$$BD = \sqrt{\left(\frac{a\varepsilon}{2} - a\varepsilon\right)^2 + \left(a\sqrt{\frac{3}{2}}\right)^2}$$

$$= \frac{a\varepsilon}{2}\sqrt{1 + \frac{3}{\varepsilon^2}} = |b_2|,$$

where a is the isotropic vortex lattice parameter and $b_1 = OB = a\varepsilon$. This means that the measurement of ratio $A/B = \eta = 1/\varepsilon = \lambda_1/\lambda_2$ of the semiaxes of the ellipse is equivalent to the description of anisotropy taken into account using the tensor of effective masses M_a and M_b.

Analysis of the geometry of vortex lattices directly from the decoration patterns is complicated by the difficulty in determining the coordinates of the centers of vortices. At the same time, Fourier patterns provide integrated (averaged) information and can easily be analyzed and processed. It follows from the relation between the direct (real) and reciprocal spaces that the ellipses drawn through the sites of a vortex lattice in the real space are similar to the ellipses drawn through Fourier maxima, but turned through 90° (Figs. 2–4). For this reason, quantitative analysis of anisotropy can be conveniently performed on a reciprocal lattice with a new basis $\mathbf{g}_1$, $\mathbf{g}_2$. If we draw an ellipse through the reciprocal lattice sites, the ratio of semiaxes will be $A^g/B^g = A/B = \eta = \lambda_1/\lambda_2$ since $\lambda \sim M^{0.5}$ [11, 12].

Here, we will try to measure anisotropic properties in the basal plane for a group of $YBa_2Cu_4O_8$ single crystals both in the superconducting state (measuring anisotropy in penetration depth) and in the normal state (resistivity measurements).

2. EXPERIMENT

We analyze the vortex structure in the basal plane of $YBa_2Cu_4O_8$ single crystals using the high-resolution decoration technique with disperse magnetic particles [13, 14]. The decoration technique involves segregation of magnetic nanoparticles at the surface of a superconductor in the regions of magnetic flux penetration at temperatures below the superconducting transition temperature T_c (5–7 K in our case). Subsequent visualization of the distribution of magnetic nanoparticle clusters (which appear as bright points in the figures below) with the help of a scanning electron microscope (SEM) gives information on the vortex structure. Decoration was carried out in a magnetic field H_e parallel to the c axis in the frozen flux regime. Information on local crystallographic orientation of the surface was obtained using the SEM in the electron channeling regime.

Single crystals were grown from Y–Ba melt under an oxygen pressure of 600–1000 bar at 1100°C [15]. Experiments were performed for a number of single

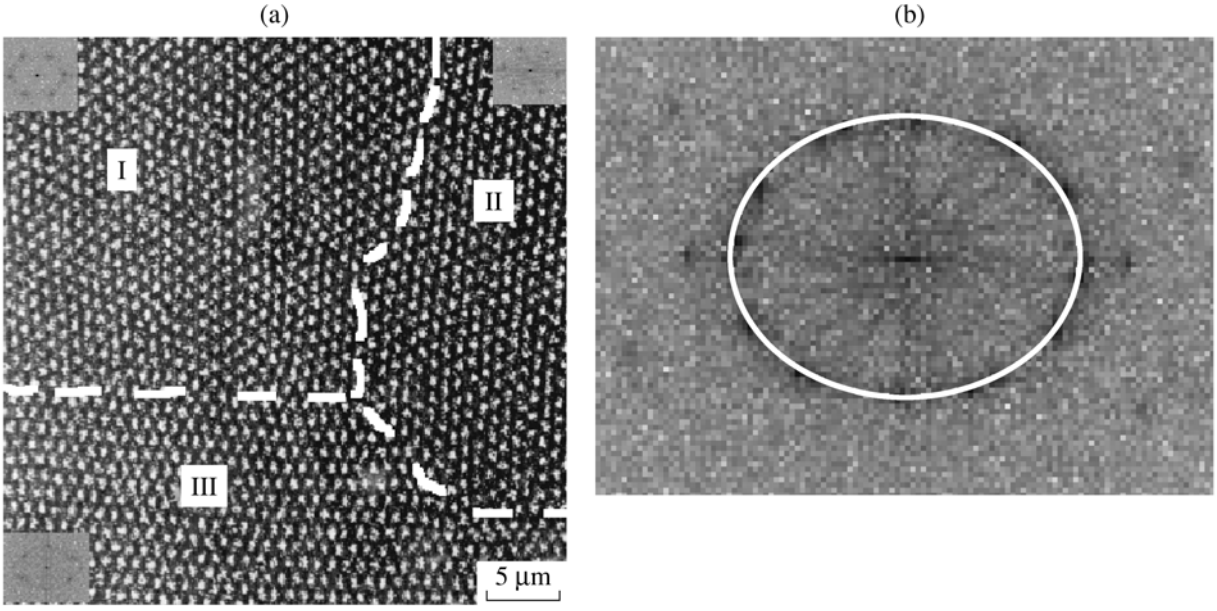

Fig. 3. (a) Domain structure in the basal plane of a $YBa_2Cu_4O_8$ single crystal in a magnetic field of 41 Oe. The insets show the Fourier transform for each domain on an arbitrary scale. (b) Fourier transform (on the arbitrary scale) of the image of the vortex lattice depicted in Fig. 3a.

crystals in a field range of 40–600 Oe. When experiments were performed on the same single crystal in different fields, magnetic particles of the previous decoration were washed out from the surface with isopropyl alcohol. It should be noted that visualization of the vortex structure using the decoration technique is hampered in fields higher than the lower critical field H_{c1} due to overlapping of the magnetic fields from individual vortices; for strongly anisotropic HTSCs, this field does not exceed approximately 100 Oe as a rule. However, this limit can be raised by an order of magnitude by optimizing the magnetic nanoparticles size and using Fourier analysis of the images.

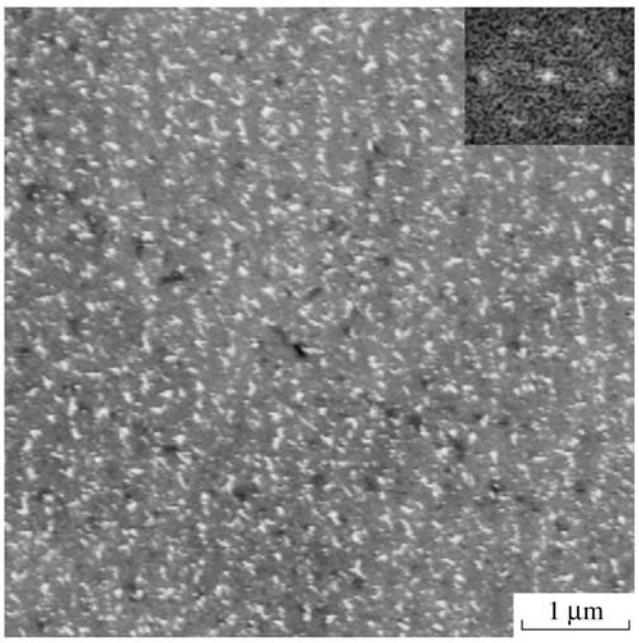

Fig. 4. Vortex structure in a magnetic field of 250 Oe. The inset shows the Fourier transform on the arbitrary scale.

Figure 2a shows the vortex lattice in the (001) basal plane in a magnetic field of 41 Oe (the inset in the right corner shows the Fourier transform of the image on an arbitrary scale). Figure 2b shows the patterns of electron channeling, indicating the local crystallographic orientation of a microscopic region of a size of approximately 100 μm^2 in the sample under investigation. A noticeable difference from a regular (60-degree) triangular lattice can clearly be seen in the Fourier pattern. In addition, it can be seen that the close packing direction in the vortex lattice is parallel to the [100] cubic axis of the single crystal and the vortex lattice is compressed in the [010] direction.

Observations of six $YBa_2Cu_4O_8$ crystals investigated here show that the vortex structure consists of domains in which the close packing directions in the vortex lattice are oriented identically relative to the axes of the single crystal. Such domains are separated by dashed curves in Fig. 3a. The insets to Fig. 3a show the corresponding Fourier transforms of three domains, while Fig. 3b shows the combined Fourier transform from three domains (for better visualization, the contrast in Fig. 3 for the Fourier transforms is inverted). We draw your attention to the fact that the close packing direction of vortices for domains I and II are close to the [100] direction, in which the vortex lattice is stretched,

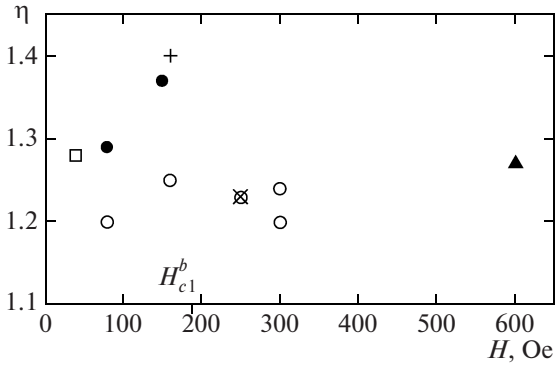

Fig. 5. Magnetic field dependence of ratio η of the semiaxes of the ellipses for six $YBa_2Cu_4O_8$ crystals marked by different symbols.

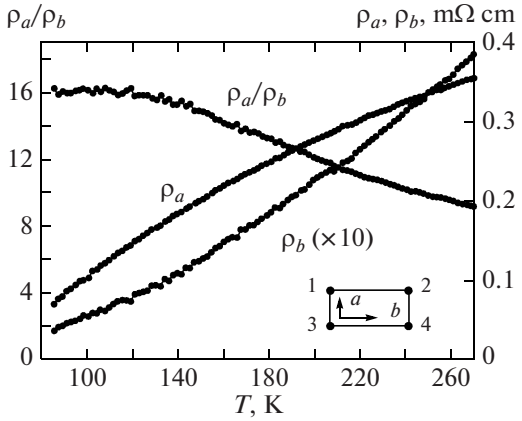

Fig. 6. Temperature dependences of resistivities ρ_a, ρ_b, and their ratio for a $YBa_2Cu_4O_8$ single crystal. The inset shows the positions of the contacts on the sample.

while the corresponding direction in domain III is turned through 90°. Figure 4 shows the vortex structure in a magnetic field of 250 Oe. In spite of strong noise contamination of the image, the Fourier transform clearly demonstrates the arrangement of Fourier peaks on the elliptic curve. Analogous patterns were observed up to a field of $H = 600$ Oe.

It is convenient to estimate the vortex lattice anisotropy quantitatively from the ratio of the semiaxes of the ellipse containing the Fourier maxima of the first or higher orders [9, 14]. Using a computer program, we determined the coordinates of three Fourier maxima and the orientation of the semiaxes relative to the cubic direction in the basal plane. For example, for the pattern depicted in Fig. 3a, the ratio of the major to minor semiaxes is $\eta = 1.37 \pm 0.05$. The orientation of the semiaxes is close to the ⟨100⟩ type directions to within a few degrees. This orientation of the ellipse semiaxes is preserved in all domains ("grains") of the vortex structure (see Fig. 3). Figure 3b clearly shows that the Fourier maxima from different domains lie on the same elliptic curve. Our measurements show that the ratio of the semiaxes is $\eta = 1.2$–1.4 for various regions in the sample and is independent of the magnetic field (Fig. 5).

Thus, our experimental observations can be interpreted as the result of anisotropy in the London penetration depth $\eta = \lambda_1/\lambda_2$ in the *ab* basal plane of the $YBa_2Cu_4O_8$ single crystal, where λ_1 and λ_2 are the penetration depths in the [100] and [010] directions, respectively. (We use notation λ_1 and λ_2 instead of λ_a and λ_b because directions **a** and **b** cannot be distinguished using the channeling pattern.) It should be noted that the value of η measured from decoration experiments in $YBa_2Cu_4O_8$ single crystals is noticeably higher than for $YBa_2Cu_3O_7$ single crystals (for which $\eta = 1.1$–1.2) [9, 16].

For electric measurements, we used a sample in the form of a thin rectangular wafer with a size of $1.2 \times 0.3 \times 0.05$ mm and with the lateral faces parallel to the crystallographic axes. The **a** and **b** axes were in the plane of the wafer, the **b** axis being parallel to its longer side. Ohmic contacts were prepared on the sample edges (see the inset to Fig. 6) by application of a silver paste with subsequent annealing at $T = 500$°C for 20 min. The contacts had characteristic sizes of 0.1–0.2 mm and were applied so that the uniform distribution of current over the sample thickness was ensured. In experiments, we measured ratios $R_a = V_{13}/J_{24}$ and $R_b = V_{12}/J_{34}$, from which components ρ_a and ρ_b of the resistivity tensor were calculated using the Montgomery technique. Figure 6 shows the $\rho_a(T)$ and $\rho_b(T)$ dependences, as well as the temperature dependence of anisotropy ρ_a/ρ_b in the plane of the sample.

It can be seen from the results depicted in Fig. 6 that the resistivity anisotropy near T_c noticeably exceeds the anisotropy in the penetration depth. It should be noted in this connection that the resistivity anisotropy is a linear function of the ratio of effective masses of charge carriers, while the ratio of penetration depths is proportional to the square root of the ratio of effective masses [11, 12].

3. DISCUSSION

Before discussing the main results, let us consider the possibility of their comparison with predictions of the theory [11, 12]. It should be noted that decoration of the vortex structure can be carried out in relatively low fields as compared to the critical field in the field cooling mode due to pinning and a large demagnetizing factor for the planar samples under investigation, for which field $\mathbf{H}_e$ is parallel to the **c** axis. For $YBa_2Cu_4O_8$ single crystals, the values of H_{c1} in the **a** and **b** directions in magnetic measurements on a single crystal with $T_c = 74$ K were indistinguishable at low temperatures (of about 10 K) and amounted to 200 Oe for a magnetic field directed along the **c** axis [17]. We can roughly estimate the values of $(H_{c1})^a$ and $(H_{c1})^b$ assuming that $(H_{c1})^b$ is the value of the field for which

the spacing between vortices is 2λ [18]. For λ_a = 80 nm, λ_b = 200 nm [6], and $H_{c1} = (\Phi_0/4\pi\lambda^2)(\ln\kappa + 0.08)$, where $\kappa = \lambda/\xi$, ξ = 4.1 nm [3], we find that $(H_{c1})^b$ = 180 Oe and $(H_{c1})_a$ = 1100 Oe. A more correct estimate of the value of H_{c1} in the basal plane, viz., $H_{c1} = (\Phi_0/4\pi\lambda_a\lambda_b)$, gives H_{c1} = 440 Oe.

Thus, our results correspond to the condition $H > (H_{c1})^b$ at least for the [100] direction and can be compared with the predictions of the theory [11]. At the same time, it can be seen from Fig. 5 that no strong variation of the anisotropy parameter is observed near $(H_{c1})^b$, which allows us to extrapolate our results to the range of stronger fields.

Theoretically [11], the orientation of the vortex lattice depicted in Fig. 2a for domains I and II is advantageous from the energy point of view; in this orientation, the major semiaxis of the ellipse in the real vortex lattice is parallel to the direction in which effective mass M_b is smaller. At the same time, it can be seen that the least advantageous orientation is observed in domain III. A possible reason for the existence of such a structure is collective pinning [10] at weak pointlike centers, which leads to violation of the long-range order in the vortex structure [18] and to the formation of a domain structure. At the same time, the shape of the unit cell of the vortex lattice in each domain is controlled by the paired interaction and anisotropy of the penetration depth ($\lambda_a \neq \lambda_b$), which is responsible for the distortion ("compression") of the regular triangular lattice (see Figs. 1 and 3b).

According to our measurements, resistivity anisotropy ρ_a/ρ_b in the basal plane at room temperature is approximately 8 and increases monotonically upon cooling, attaining a value of 16 in the vicinity of the superconducting transition. These values are noticeably higher than those obtained in [1–3]. A possible reason for such a discrepancy may be the difference in the geometry of contacts. Indeed, when resistivity anisotropy was measured in the plane of the wafer using the Montgomery method [19], the current was assumed to be distributed uniformly over the sample thickness. However, the contacts in [1–3] were deposited on the plane surface of the wafer near its corners, which must lead to violation of this condition. Since the value of ρ_c is considerably higher than ρ_a and ρ_b, the current passed through the contacts prepared on the *ab* plane is concentrated at the surface; the higher the anisotropy, the stronger the effect is manifested. The inequality $\rho_a > \rho_b$ leads to $\rho_c/\rho_a < \rho_c/\rho_b$; i.e., when contacts on the *ab* plane are used, the current directed along the **b** axis is "pressed to the surface" more strongly than the current directed along the **a** axis. As a result, the resistivity measured along the **b** axis is higher than the resistivity measured along **a**, the difference being larger than in the case of a uniform distribution of the current over the wafer thickness; consequently, such measurements give a lower value of anisotropy ρ_a/ρ_b. Estimates based on the formulas from [20] show that the apparent value of anisotropy $(\rho_a/\rho_b)^*$ obtained for a nonuniform distributions of current over the thickness of a rectangular sample with contacts located on the *ab* plane is $(\rho_a/\rho_b)^* \approx (\rho_a/\rho_b)^{1/2}$. The results of our measurements and the data obtained in [1–3] closely satisfy the same relation. Thus, we can admit the discrepancy with the available data [1–3], but not with the main effect: a considerable discrepancy between the anisotropy parameters calculated from the resistive measurements and from the vortex lattice parameters (penetration depth anisotropy). Indeed, if anisotropy ρ_a/ρ_b is controlled by the ratio M_a/M_b of effective masses, we have ρ_a/ρ_b = 16 near T_c. Since $\lambda \sim M^{0.5}$ [11, 12], we have $(M_a/M_b)^{0.5} = 4$, which strongly differs from the value of η = 1.3 measured from the vortex lattice geometry. The reason for this discrepancy may be the difference in determining the effective mass from the data on resistivity and penetration depth [22, 23]. It is well known that the reciprocal effective mass tensor in the band theory is $(m^*)^{-1} = \partial^2 E/\partial p_i \partial p_j$, while the effective mass tensor in the Ginzburg–Landau anisotropic equations has the form [23, 24]

$$(m^*)^{-1} = \frac{7\zeta(3)}{12\pi^2 T_c}\langle v_i v_j \psi^2 \rangle,$$

where v_i and v_j are the velocities averaged over the Fermi surface and ψ is the order parameter. The difference in determining the effective mass becomes significant in the dirty limit $l < \xi$ (l is the mean free path and ξ is the coherence length in the basal plane) [22]. The value of the mean free path estimated from the resistivity of the crystals under investigation is closer to a dirty limit of $l \approx 4$ nm. Experiments with cleaner crystals and detailed analysis of the Fermi surface in $YBa_2Cu_4O_8$ crystals will probably help in solving the problem of the difference in anisotropy defined using the concept of effective masses of carriers in the normal and superconducting states.

ACKNOWLEDGMENTS

The authors are grateful to N.S. Sidorov, who prepared the contacts, and to V.G. Kogan and V.V. Ryazanov for fruitful discussions.

This study was supported financially by the Russian Foundation for Basic Research (project no. 07-02-00174) and as part of the program "Properties of Condensed Media" of the Presidium of the Russian Academy of Sciences.

REFERENCES

1. B. Bucher, J. Karpinski, E. Kaldis, and P. Wachter, J. Less-Common Met. **164/165**, 20 (1990).
2. J. Schoenes, J. Karpinski, E. Kaldis, J. Keller, and P. de la Mora, Physica C (Amsterdam) **166**, 145 (1990).
3. B. Bucher, J. Karpinski, E. Kaldis, and P. Wachter, Physica C (Amsterdam) **167**, 324 (1990).

4. B. Bucher, P. Steiner, J. Karpinski, E. Kaldis, and P. Wachter, Phys. Rev. Lett. **70**, 2012 (1993).
5. Kuan Zhang, D. A. Bonn, S. Kamal, R. Liang, D. J. Baar, W. N. Hardy, D. Basov, and T. Timusk, Phys. Rev. Lett. **73**, 2484 (1994).
6. D. N. Basov, R. Liang, D. A. Bonn, W. N. Hardy, B. Dabrowski, M. Quijada, D. B. Tanner, J. P. Rice, D. M. Ginsberg, and T. Timusk, Phys. Rev. Lett. **74**, 598 (1995).
7. V. N. Molchanov, M. K. Blomberg, M. Yu. Merisalo, and V. I. Simonov, Pis'ma Zh. Éksp. Teor. Fiz. **66** (7), 502 (1997) [JETP Lett. **66** (7), 534 (1997)].
8. R. Khasanov, T. Schneider, R. Brütsch, D. Gavillet, J. Karpinski, and H. Keller, Phys. Rev. B: Condens. Matter **70**, 144 515 (2004).
9. L. Ya. Vinnikov, I. V. Grigorieva, L. A. Gurevich, and Yu. A. Osip'yan, Pis'ma Zh. Éksp. Teor. Fiz. **49** (2), 83 (1989) [JETP Lett. **49** (2), 99 (1989)].
10. A. I. Larkin and Yu. N. Ovchinnikov, Zh. Éksp. Teor. Fiz. **65** (4), 1704 (1973) [Sov. Phys. JETP **38** (4), 854 (1973)].
11. L. J. Campbell, M. M. Doria, and V. G. Kogan, Phys. Rev. B: Condens. Matter **38**, 2439 (1988).
12. G. Blatter, M. V. Feigel'man, V. B. Geshkenbein, A. I. Larkin, and V. M. Vinokur, Rev. Mod. Phys. **66**, 1125 (1994).
13. U. Essmann and H. Träuble, Phys. Lett. A **54**, 596 (1967).
14. L. Ya. Vinnikov, I. V. Grigor'eva, and L. A. Gurevich, in *The Real Structure of High-T_c Superconductors*, Ed. by V. Sh. Shekhtman (Springer, Berlin, 1993), p. 89.
15. J. Karpinski, G. I. Meijer, H. Schwer, R. Molinski, E. Kopnin, K. Conder, M. Angst, J. Jun, S. Kazakov, A. Wisniewski, R. Puzniak, J. Hofer, V. Alyoshin, and A. Sin, Supercond. Sci. Technol. **12**, R153 (1999).
16. G. J. Dolan, F. Holtzberg, C. Feild, and T. R. Dinger, Phys. Rev. Lett. **62**, 2184 (1989).
17. J. C. Martinez, J. J. Prèjean, J. Karpinski, E. Kaldis, and P. Bordet, Solid State Commun. **75**, 315 (1990).
18. V. V. Schmidt, *The Physics of Superconductors: Introduction to Fundamentals and Applications* (Nauka, Moscow, 1982; Springer, Berlin, 2002).
19. A. I. Larkin, Zh. Éksp. Teor. Fiz. **58**, 1466 (1970) [Sov. Phys. JETP **31**, 784 (1970)].
20. H. C. Montgomery, J. Appl. Phys. **42**, 2971 (1971).
21. L. I. Buravov, Zh. Tekh. Fiz. **64** (7), 200 (1994) [Tech. Phys. **39** (7), 743 (1994)].
22. A. A. Varlamov and A. I. Larkin, *Theory of Fluctuations in Superconductors* (Dobrosvet, Moscow, 2007; Oxford University Press, Oxford, 2009).
23. L. P. Gor'kov and T. K. Melik-Barkhudarov, Zh. Éksp. Teor. Fiz. **45**, 1493 (1963) [Sov. Phys. JETP **18**, 1031 (1963)].
24. L. P. Gor'kov and D. Jerome, J. Phys., Lett. **46**, L-643 (1985).

Translated by N. Wadhwa